ELSEVIER

Earth and Planetary Science Letters 5707 (2000) 1–9

EPSL

www.elsevier.com/locate/epsl

Phase stability and density of FeS at high pressures and temperatures: implications for the interior structure of Mars

Abby Kavner [a,1], Thomas S. Duffy [a,*], Guoyin Shen [b]

[a] *Department of Geosciences, Princeton University, Princeton, NJ 08544, USA*
[b] *Consortium for Advanced Radiation Sources, University of Chicago, Chicago, IL 60637, USA*

Received 4 April 2000; received in revised form 16 November 2000; accepted 20 November 2000

Abstract

The phase diagram of stoichiometric iron sulfide (FeS) was investigated at high pressures and temperatures (15–35 GPa, 1400–2200 K) with a laser-heated diamond anvil cell and synchrotron X-ray diffraction. The NiAs-structured polymorph of FeS is found to be stable within the *P-T* range of the Martian core. The density of FeS at 1600 K is measured to be 5.96 g/cm^3 at 17 GPa and 6.65 g/cm^3 at 35 GPa. The density measurements are used to evaluate structural models of Mars containing a core within the Fe–FeS system. The models that satisfy the geophysical constraints proscribe limits on the thickness of the Martian crust, the size and composition of the core, and the thickness of a perovskite-bearing layer close to the Martian core–mantle boundary.

1. Introduction

Understanding a planet's structure and evolution requires combining geophysical observations (e.g., seismic and gravity data) with measurements on candidate materials at conditions relevant to the planetary interior. The interpretation of recent advances in our understanding of Martian geophysics [1–3], and possible future Martian seismological exploration [4], requires information on the phase stability and density of core constituents at the high pressure and temperature (*P-T*) conditions of the Martian core. Iron alloys are believed to be the principal constituent of terrestrial planets' cores, and sulfur is likely to be a major alloying component of the Martian core based on its abundance in SNC meteorites, theoretical models of nebular condensation, and its ability to dissolve into liquid iron [5,6].

There has been extensive interest in the high *P-T* behavior of stoichiometric iron sulfide (FeS) because it undergoes a series of structural and electronic phase transformations with increasing pressure and temperature in the range of 0–25 GPa [7–11] and 300–800 K [12,13]. The stable form at ambient pressure and temperature is troilite, a superstructure of the NiAs structure with cell constants ($\sqrt{3}a$, $2c$), where a, c are the cell constants of the NiAs structure. At room temperature and pressures above 7 GPa, troilite transforms to a monoclinic structure related to the

* Corresponding author. Tel.: +1-609-258-6769; Fax: +1-609-258-1274; E-mail: duffy@geo.princeton.edu

[1] Now at Lamont-Doherty Earth Observatory, 61 Rt. 9W, Palisades, NY 10964, USA.

0012-821X/00/$ – see front matter
PII: S0012-821X(00)00356-3

MnP form, FeS III [8,10,12,13]. Above 7 GPa, FeS III transforms with increasing temperature first to a (2*a,c*) hexagonal superstructure of the NiAs structure, FeS IV, and then to the NiAs structure, FeS V [12,13]. However, because of uncertainties in extrapolating, the stable phase and equation of state of FeS at the conditions of the terrestrial planets' cores remains unknown. Recent advances in X-ray diffraction coupled with double-sided laser heating in the diamond anvil cell [14] now allow direct measurements of materials at the high *P-T* conditions relevant to the Martian core. In this study, we examined the structure and density of FeS at extreme conditions using X-ray diffraction in a laser-heated diamond anvil cell.

2. Experiment

Experiments were performed at the undulator beamline (13-ID-D) of the GSECARS sector of the Advanced Photon Source. Synthetic, stoichiometric FeS [12] was loaded in a symmetric diamond anvil cell and sandwiched between layers of MgO which served as a thermal insulator and pressure calibrant. To minimize axial temperature gradients, samples were heated from both sides simultaneously with a Nd:YLF laser [14]. To measure temperature, spectral intensity of the thermal radiation was collected from both sides of the sample, dispersed by an imaging spectrometer and recorded on a CCD. Temperatures were determined by fitting the spectral intensity, corrected for the system response, to Wien's approximation to Planck's law [15] (Fig. 1). Temperature as a function of distance across the hotspot was determined with a spatial resolution of about 1.7 μm.

Energy-dispersive X-ray diffraction patterns ($2\theta = 5.5°$) were recorded before heating, at 1–2 min intervals during heating, and after thermal quenching. Special care was taken to ensure the alignment of the X-ray beam (10×10 μm) within the laser-heated spot (hotspot width ~ 20 μm): the size of the X-ray beam was determined by scanning a sharp edge across the beam, and the diameter of the heating spot (Fig. 1) was determined from the FWHM of the measured spectral intensity profile. Both sides of the sample were also visually monitored during heating using CCD cameras. Five heating cycles were performed on two separate samples of FeS.

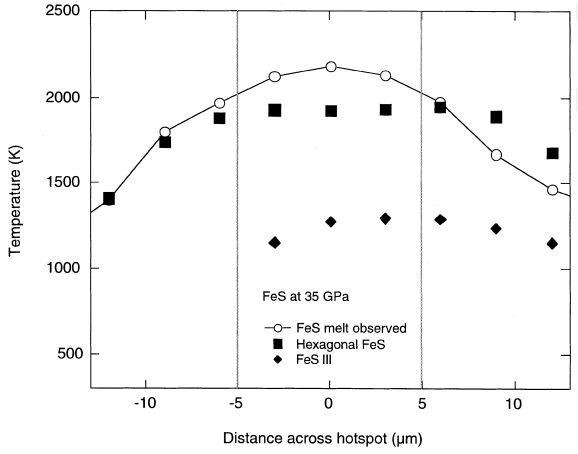

Fig. 1. Measured temperature profiles of FeS at 35 GPa. Each point is the temperature determined from a fit to Wien's approximation to Planck's law across the hotspot. Circles are temperatures measured from a sample that appeared to be molten, and showed no diffracted intensity. Squares denote a temperature profile from the hexagonal FeS sample. Diamonds depict the highest temperatures at which diffraction patterns indicated the presence of FeS III. Vertical gray lines show the X-ray beam width. The precision of each temperature measurement is within the size of the symbols.

The pressure inside the sample chamber was determined from the (200) reflection of MgO and its room temperature non-hydrostatic equation of state [16]. The presence of deviatoric stress, and its change during heating can introduce an error in the pressure calibration of 5–10% [17]. In addition, temperature gradients within the MgO insulating layer during heating may result in a pressure underestimate of 1–2 GPa [18].

3. High *P-T* phase diagram of FeS

The heating cycle at 35 GPa (Fig. 2) shows the presence of two phase transformations in FeS. At the peak temperature, visual observation of the FeS revealed rapid textural changes indicative of fluid flow associated with melting [18]. The corre-

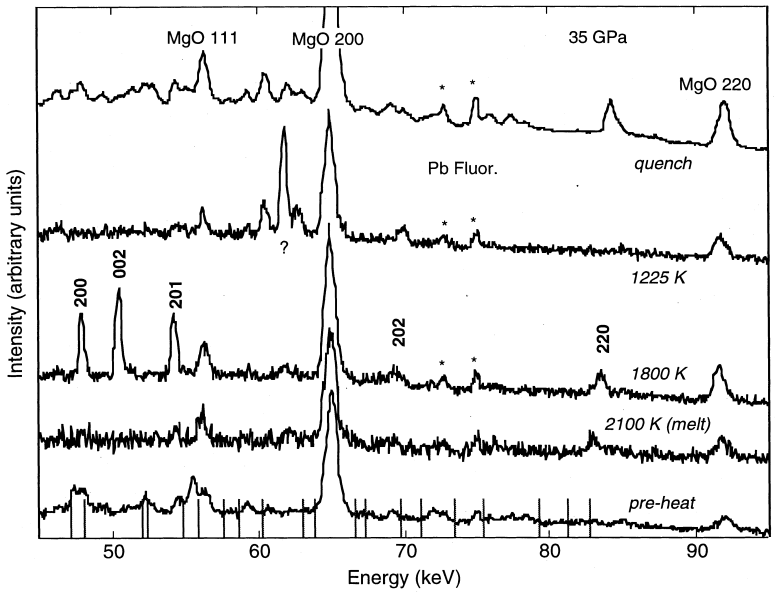

Fig. 2. Diffraction patterns from FeS heating cycle at 35 GPa, as a function of energy. The temperature corresponding to the X-ray volume is indicated alongside each pattern. The pattern at 2100 K was collected for ~1 min, the other high temperature patterns for ~5–10 min. The quench pattern was exposed for several hours. MgO, hexagonal FeS, and fluorescence lines are labeled. Vertical lines show the room temperature positions of FeS III [13].

sponding diffraction pattern showed only peaks due to the MgO insulation layer. As the sample temperature was lowered, peaks indicating the presence of hexagonal FeS appeared, including the (200), (002), and (201) triplet. The appearance of hexagonal FeS under cooling conditions suggests that the crystals nucleated from the FeS melt, providing a strong confirmation of the thermodynamic stability of the hexagonal phase at these conditions. As the sample temperature was lowered further, the hexagonal peaks disappeared, and were replaced by diffraction lines consistent with FeS III. The 300 K diffraction patterns both before and after heating are also consistent with the presence of FeS III [10,12,13].

This data set displayed excellent coupling of the laser on each side of the FeS sample, and the hotspot was well aligned within the X-ray diffraction beam (Fig. 1). The high precision of each temperature measurement (~5–20 K) results from the excellent fit of the spectral intensity to Wien's approximation to Planck's law. The accuracy of the temperature is much more difficult to interpret. For example, temperature fluctuations over the time period in which the diffraction patterns are collected are estimated to be of the order of ~100 K for these experiments, based on several temperature measurements at a single laser power. A second issue is that the temperature gradient must be measured and compared with the X-ray spot size to determine the average temperature over the diffracting volume. The corrected temperatures may be lower than the peak hotspot temperatures by 100–300 K [18]. Finally, the graybody assumption may create systematic errors of the order of 200–300 K in either direction if the emissivity of FeS has a wavelength dependence in the visible range [20].

The data set from this heating cycle thus constrains the phase boundaries of FeS at 35 GPa from room temperature to melting. We observed melting at 2100(100) K, consistent with the melting curve reported by Boehler [21]. The FeS III–hexagonal FeS boundary was determined to be 1225(35) K, indicating that phase III persists to higher temperatures than expected based on extrapolation of low *P-T* data [12,13]. Interestingly, the diffraction data indicate that FeS III trans-

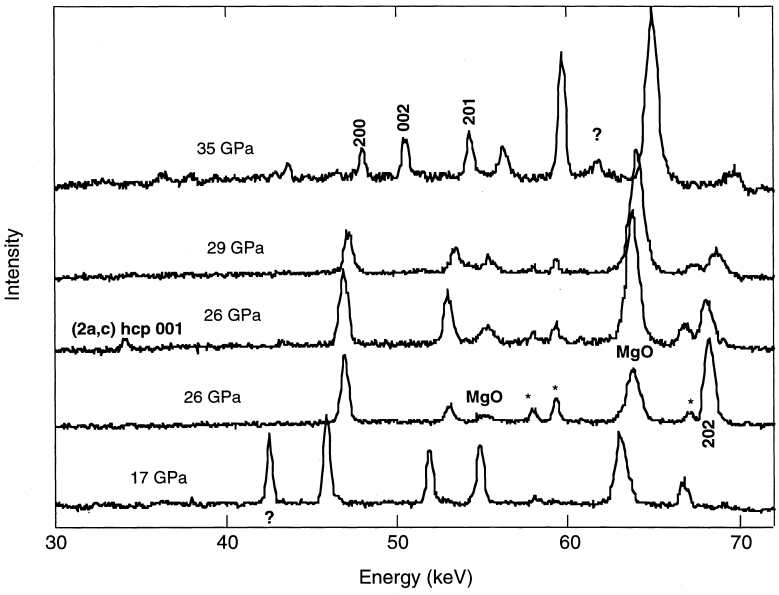

Fig. 3. High temperature diffraction patterns for each heating cycle plotted as a function of energy. The positions of the hexagonal (200), (002), (201), and (220) peaks, as well as the (2*a,c*) (001) superlattice reflection are shown. MgO peaks are also indicated. Asterisks indicate intensity due to Pb fluorescence. Patterns were collected for ~10 min.

forms directly to the FeS V phase at 35 GPa. Unfortunately, the difficulty in achieving and measuring temperatures lower than ~1200 K in FeS using the laser heating system precluded measurements of the FeS III–hexagonal boundary at lower pressures.

The high temperature diffraction patterns (Fig. 3) reveal the presence of FeS V, and possibly FeS IV, throughout the conditions of the Martian core (Fig. 4). Each is a time-integrated diffraction pattern (10–20 min) during a single cycle at temperatures ranging from 1400 to 1800 K. To evaluate the effect of collecting a diffraction pattern for a wide temperature range, we can compare the long exposure data to the diffraction patterns obtained at shorter time intervals (1–2 min). Because of lattice shifts due to thermal expansion, we would expect the longer time diffraction patterns to display broader diffraction lines. However, the measurements indicate that this broadening is a small effect: for example, the data set at 26 GPa (center pattern in Fig. 3) results from adding together several 1–2 min diffraction patterns. In the summed diffraction pattern, the line widths of the (200) and (201) hexagonal FeS lines are 292 and 375 eV, while the corresponding line widths of the six contributing patterns average 291 ± 13 and 348 ± 48 eV (error bars are standard deviations). Thus, time-integrating the high temperature diffraction patterns causes negligible error, increases the signal-to-noise ratio, and helps minimize the effects of preferred orientation, thereby yielding a high precision volume measurement over a temperature range directly relevant to the Martian core.

All observed high temperature peaks can be attributed to FeS, MgO, or fluorescence lines except for a peak at 42.5 keV at 17 GPa, and another at 61.8 keV at 35 GPa. The origins of these lines are unknown, but each only appeared in no more than two time-adjacent diffraction patterns, suggesting that they might represent a minor impurity phase exhibiting a high degree of preferred orientation. All but one of the patterns can be indexed as the NiAs structure (FeS V); only the pattern at 26 GPa showed evidence of the superlattice peak (001) corresponding to the distorted (2*a,c*) NiAs cell (FeS IV). Our results thus rule

out Fei et al.'s [12] suggestion that FeS in the Martian core will be wholly in the stability field of phase IV, but are consistent with Kusaba et al.'s [13] extrapolation of their measured FeS IV–V boundary (Fig. 4).

In addition to extending the phase diagram of Fe to higher pressures and temperatures, we also determine the unit cell parameters of FeS at high *P-T* conditions. From a technical standpoint, comparing measurements from different high *P-T* studies is an important cross-check, establishing the mutual reliability of techniques used to measure material properties at ultra-high pressures and temperatures. To facilitate comparison with previous data, both hexagonal polymorphs (FeS IV and FeS V) were indexed on the basis of the doubled (2*a,c*) unit cell. Hexagonal cell parameters calculated from the diffraction patterns (Fig. 5) are in agreement with previous results [12,13]. Our data also demonstrate (Fig. 5, inset) that the *c/a* ratio tends to increase away from its ideal value in our experiments, which are at higher pressures and temperatures than the previous experiments.

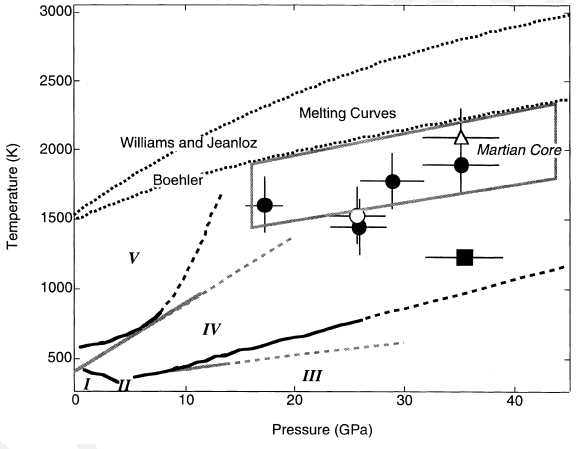

Fig. 4. Phase diagram of FeS. Solid circles indicate the presence of (*a,c*) hexagonal FeS (V), while the open circle shows (2*a,c*) FeS (IV). The filled square indicates the highest temperature at which FeS III is observed. The open triangle indicates FeS melting. Lower *P-T* phase boundaries are shown as black [12] and gray [13], with their extrapolations shown as dashed extensions. Experimentally determined melting curves of FeS are also shown [21,36]. Plausible temperature ranges for the Martian core are represented by the boxed region [2].

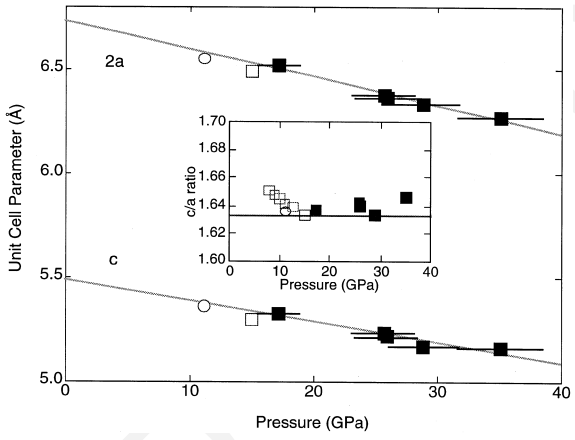

Fig. 5. Unit cell parameters (2*a,c*) of FeS at high temperatures as a function of pressure (filled squares). The inset shows the *c/a* ratio calculated from these data. Also shown are data from Fei et al. [12] (open squares) and Kusaba et al. [13] (open circles) at temperatures of 600–623 K and 573 K, respectively. The linear fit is for the present data set only.

4. Martian structure models

Our new high *P-T* measurements of the density of FeS enable refinement of models of the interior structure of Mars based on direct measurements of the properties of its core constituents at the relevant temperatures and pressures. Models for the structure and chemistry of the Martian interior are based on interpretation of several lines of evidence: the geochemistry of meteorites of Martian origin [6], cosmochemical models for the accretion of terrestrial planets [5], phase stability and element partitioning of candidate mineral assemblages [22–24] and the geophysical constraints of mass and polar moment of inertia [1]. The estimate for the composition of the Martian core based on partitioning experiments combined with data for Martian meteorite geochemistry [6] yields an iron core with 14–17% sulfur, a number commonly cited for the Martian core composition (e.g., [2]). However, geochemical estimates of the composition of the Martian core span a wide range, with estimates for sulfur contents as low as 0.4% [24].

Using our experimental measurements of the density of hexagonal FeS at Martian core conditions (Fig. 6) and volumes of γ-Fe measured

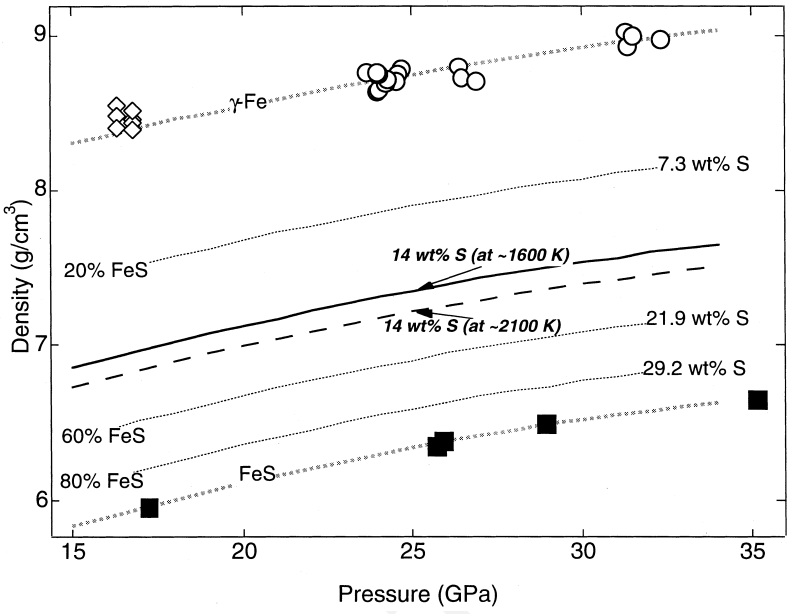

Fig. 6. Density of FeS (solid squares) and Fe (open diamonds [25] and open circles [26]) as a function of pressure at 1675(250) K for FeS and 1300–1600 K for Fe. Best-fit curves through each data set are shown as dotted gray lines. Thin solid lines show density contours of an ideal mixture of Fe and FeS, labeled in mol% FeS and wt% S. The black line shows the density contour calculated for a mixture containing 14 wt% S [6]. The thick black dotted line shows the density change resulting from a 500 K increase in temperature at 14 wt% S content.

under similar conditions [25,26] as endmembers, we calculated the density of Fe–FeS mixtures in the pressure range of 15–40 GPa at an average temperature of 1600(250) K. Possible intermediate compounds within the Fe–FeS system are expected to have only a small effect on the calculated density [27]. To illustrate how temperature changes affect density, we assume an average thermal expansion of 4×10^{-5} K^{-1} and find that a 500 K temperature increase results in a density decrease of less than 2%, equivalent to the density difference between 14 wt% S and 16 wt% S. This difference does not significantly affect the model results. In addition, depending on the core temperature and sulfur content, liquid iron sulfide may be present. Measurements of the density of liquid Fe–S compositions [28] are at much lower pressures and different compositions, making a direct comparison difficult. However, since the concave-downward shape of the FeS melting curve (Fig. 4) suggests that the ΔV_{s-l} becomes less pronounced with increasing pressure, we do not expect the presence of partial melt to significantly change the results of the interior structure models.

We constructed a series of models of the density of the Martian interior, assuming an Fe–FeS core (Fig. 7). We used a density profile for the Martian mantle determined by Bertka and Fei [29]. For a given crustal thickness and density, the core radius and/or sulfur content was adjusted to satisfy the Martian mass constraint, and the model's polar moment of inertia was calculated and compared with the most recent value from Mars Pathfinder data [1]. The bulk composition (Fe/Si or total Fe) was not constrained in our model. We find that a wide range of models can satisfy existing constraints (Fig. 7). Assuming an average crustal thickness of 50 km, the core mass fraction ranges from 11.8 to 19.3% as the composition is varied from pure Fe to pure FeS. For a core containing 14 wt% S [6], the core mass fraction and radius are 15.4% and 1480 km, respectively. While these conclusions are generally in agreement with previous results [29–33], the fact that the present study is based on densities measured directly

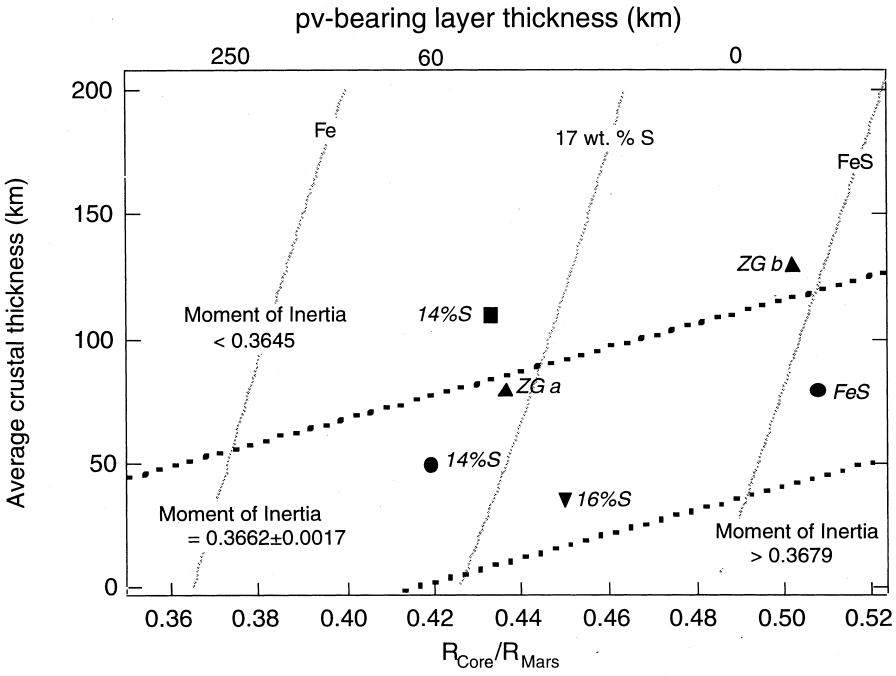

Fig. 7. Interior structure models for Mars. Thick dotted lines constrain the range of acceptable models. Thin dotted lines show the range of solutions for a given core sulfur content. The figure illustrates the tradeoff between the allowable average crust thickness and the density and radius of the core. The thickness of the perovskite layer is indicated on the top axis. Previous estimates are also depicted as follows: open circles with sulfur contents labeled [30]; open squares [2]; downward triangles [36]; upward triangles [35] (core sulfur content not calculated).

under Martian core *P-T* conditions places these conclusions on much firmer ground.

The model results are especially sensitive to the thickness and composition of the Martian crust (Fig. 7) [29]. Changing the average crust thickness from 50 to 200 km decreases the moment of inertia by 0.0069, corresponding to a 4σ change. Mars is characterized by a well-known crustal dichotomy and estimates for the average crustal thickness based on gravity, petrologic, and geochemical data range from ~20 to ~200 km [3,33,34]. Our results strictly disallow Martian models with a crust thicker than 125 km, and favor a much lower crustal thickness, consistent with Zuber et al.'s [3] estimate of a 50 km average crustal thickness for Mars. Recent geochemical models suggesting an almost pure iron core for Mars [24] would further constrain the average crustal thickness to be less than 50 km.

In Mars, the transformation of mantle silicates to the dense perovskite phase assemblages occurs very close to its core–mantle boundary. Because a perovskite-bearing layer will contribute a thermal boundary layer in the deep mantle, it plays an important role in regulating the thermal and convective development of the Martian interior [35]. For example, the presence of such a layer may increase Martian core temperatures, thus increasing the potential for a convecting liquid phase driving an early Martian dynamo. Fig. 7 shows the tradeoffs between core radius, density, and crustal thickness in determining the presence of a perovskite layer. The thicker (or less dense) the crust, the less likely a perovskite layer exists in the lower mantle.

The nature of both the crust and the core–mantle boundary may have important implications for volcanism and dynamic history of Mars, and for the thermal history and state of the Martian interior. The models resulting from our present experimental results show how the addition of a single piece of information – either the size of

the core, its composition, or the thickness and density of the crust – has the potential to significantly enrich our understanding of the planet from crust to core. This important additional constraint could be provided by future seismic exploration of Mars.

Because its complete *P-T* range is experimentally accessible, Mars may play a role as a crucible for examining how evidence from geophysics, geochemistry, and mineral physics combines to provide an understanding of a terrestrial planet. These results demonstrate in detail the tradeoffs between the structure and composition of a planet's crust, mantle, and core, and highlight the interdependence of geochemical, geological, and geophysical models of a terrestrial planet.

5. Uncited references

[19]

Acknowledgements

We thank Y. Fei for providing sample material and for useful discussions. We also thank W. Panero and S. Shim for discussion and experimental assistance. Portions of this work were performed at GeoSoilEnviroCARS (GSECARS), Sector 13, Advanced Photon Source at Argonne National Laboratory. GSECARS is supported by the National Science Foundation – Earth Sciences, Department of Energy – Geosciences, W.M. Keck Foundation, and the United States Department of Agriculture. Use of the Advanced Photon Source was supported by the U.S. Department of Energy, Basic Energy Sciences, Office of Energy Research, under Contract No. W-31-109-Eng-38. This work was supported by the NSF.*[FA]*

References

[1] W.M. Folkner, C.F. Yoder, D.N. Yuan, E.M. Standish, R.A. Preston, Interior structure and seasonal mass redistribution of Mars from radio tracking of Mars Pathfinder, Science 278 (1997) 1749–1752.

[2] T. Spohn, F. Sohl, D. Breuer, Mars, Astron. Astrophys. Rev. 8 (1998) 181–235.

[3] M. Zuber et al., Internal structure and early thermal evolution of Mars from Mars global surveyor topography and gravity, Science 287 (2000) 1788–1793.

[4] A. Mocquet, P. Vacher, O. Grasset, C. Sotin, Theoretical seismic models of Mars: The importance of the iron content of the mantle, Planet. Space Sci. 44 (1996) 1251–1268.

[5] A.E. Ringwood, On the Origin of the Earth and Moon, Springer Verlag, New York, 1979.

[6] G. Dreibus, H. Wanke, Mars: A volatile-rich planet, Meteoritics 20 (1985) 367–382.

[7] H.K. Mao, G. Zou, P.M. Bell, Experiments bearing on the Earth's lower mantle and core, Carnegie Inst. Washington Yearbook 80 (1981) 267–272.

[8] H.E. King, C.T. Prewitt, High-pressure and high-temperature polymorphism of iron sulfide (FeS), Acta Crystallogr. 38 (1982) 1877–1887.

[9] J.-P. Rueff et al., Pressure-induced high-spin to low-spin transition in FeS evidenced by X-ray emission spectroscopy, Phys. Rev. Lett. 82 (1999) 3284–3287.

[10] R.J. Nelmes, M.I. McMahon, S.A. Belmonte, J.B. Parise, Structure of the high-pressure phase III of iron sulphide, Phys. Rev. B 59 (1999) 9048–9052.

[11] S. Takele, G.R. Hearne, Electrical transport, magnetism, and spin-state configurations of high-pressure phases of FeS, Phys. Rev. B 60 (1999) 4401–4403.

[12] Y. Fei, C.T. Prewitt, H.K. Mao, C.M. Bertka, Structure and density of FeS at high pressure and high temperature and the internal structure of Mars, Science 268 (1995) 1892–1894.

[13] K. Kusaba, Y. Syono, T. Kikegawa, O. Shimomura, Structures and phase equilibria of FeS under high pressure and temperature, in: Properties of Earth and Planetary Materials at High Pressure and Temperature, AGU, Washington, DC, 1998, pp. 297–305.

[14] G. Shen, M.L. Rivers, S.R. Sutton, A laser heated diamond cell system at the Advanced Photon Source for in situ X-ray measurement at high pressure and temperature, Rev. Sci. Instrum. (2000) in press.

[15] R. Jeanloz, D.L. Heinz, Temperature measurements in the laser-heated diamond cell, in: M.H. Manghnani, Y. Syono (Eds.), High-Pressure Research in Mineral Physics, Terra Scientific, Tokyo, 1987, pp. 113–127,.

[16] T.S. Duffy, R.J. Hemley, H.K. Mao, Equation of state and shear strength at multimegabar pressures: magnesium oxide to 227 GPa, Phys. Rev. Lett. 74 (1995) 1371–1374.

[17] A. Kavner, T.S. Duffy, Pressure-volume-temperature paths in the laser-heated diamond anvil cell, J. Appl. Phys. (2000) in press.

[18] A. Kavner, T.S. Duffy, D.L. Heinz, G. Shen, Eos, Trans. AGU, 1998.

[19] R. Jeanloz, A. Kavner, Laser heating and imaging spectroradiometry in the diamond anvil cell, Phil. Trans. R.

Soc. London A, Math. Phys. Eng. Sci. 384 (1996) 1279–1305.
[20] A. Kavner, R. Jeanloz, The melting curve of platinum, J. Appl. Phys. 83 (1998) 7553–7559.
[21] R. Boehler, Melting of the Fe–FeO and the Fe–FeS systems at high pressure: Constraints on core temperatures, Earth Planet. Sci. Lett. 111 (1992) 217–227.
[22] J. Longhi, E. Knittle, J.R. Holloway, H. Wanke, The bulk composition, mineralogy and internal structure of Mars, in: H.H. Kieffer, B.M. Jakosky, C.W. Snyder, M.S. Matthews (Eds.), Mars, University of Arizona Press, Tucson, AZ, 1992, pp. 184–208.
[23] C.M. Bertka, Y. Fei, Mineralogy of the Martian interior up to core–mantle boundary pressures, J. Geophys. Res. 102 (1997) 5251–5264.
[24] G.A. Gaetani, T.L. Grove, Partitioning of moderately siderophile elements among olivine, silicate melt, and sulfide melt: constraints on core formation in the Earth and Mars, Geochim. Cosmochim. Acta 61 (1997) 1829–1846.
[25] R. Boehler, N. von Bargen, A. Chopelas, Melting, thermal expansion, and phase transitions of iron at high pressures, J. Geophys. Res. 95 (1990) 21731–21736.
[26] N. Funamori, T. Yagi, T. Uchida, High pressure and high temperature in situ X-ray diffraction study of iron to above 30 GPa using MA8-type apparatus, Geophys. Res. Lett. 23 (1996) 953–956.
[27] Y. Fei, C.M. Bertka, Eos, Trans. AGU, 1999.
[28] C. Sanloup, F. Guyot, P. Gillet, G. Fiquet, M. Mezouar, I. Martinez, Density measurements of liquid Fe–S alloys at high pressure, Geophys. Res. Lett. 27 (2000) 811–814.
[29] C.M. Bertka, Y. Fei, Density profile of an SNC model Martian interior and the moment-of-inertia factor of Mars, Earth Planet. Sci. Lett. 157 (1998) 79–88.
[30] C.M. Bertka, Y. Fei, Implications of Mars Pathfinder data for the accretion history of the terrestrial planets, Science 281 (1998) 1838–1840.
[31] C. Sanloup, A. Jambon, P. Gillet, A simple chondritic model of Mars, Phys. Earth Planet. Interact. 112 (1999) 43–54.
[32] V.N. Zharkov, T.V. Gudkova, Interior structure models, Fe/Si ratio and parameters of figure for Mars, Phys. Earth Planet. Interact. 117 (2000) 407–420.
[33] F. Sohl, T. Spohn, The interior structure of Mars: Implications from SNC meteorites, J. Geophys. Res. 102 (1997) 1613–1635.
[34] M.C. Norman, The composition and thickness of the crust of Mars estimated from rare earth elements and neodymium-isotopic compositions of Martian meteorites, Meteorit. Planet. Sci. 34 (1999) 439–449.
[35] H. Harder, Phase transitions and the three-dimensional planform of thermal convection in the Martian mantle, J. Geophys. Res. 103 (1998) 6775–6797.
[36] Q. Williams, R. Jeanloz, Melting relations in the iron–sulfur system at ultra-high pressures: implications for the thermal state of the Earth, J. Geophys. Res. 95 (1990) 19299–19310.